

Lect. 3 Digital Recording and Numerical Reconstruction of Holograms**3.1. Introduction**

First experiments in numerical reconstruction of optical holograms date back to 1960-70-th ([1-3]). At that time, scanning devices that could be used for digitizing holograms, had low resolution, which required optical magnification of holograms to fit them to the resolution of scanning devices. Fig. 3.1 reproduces the result reported in [1, 2].

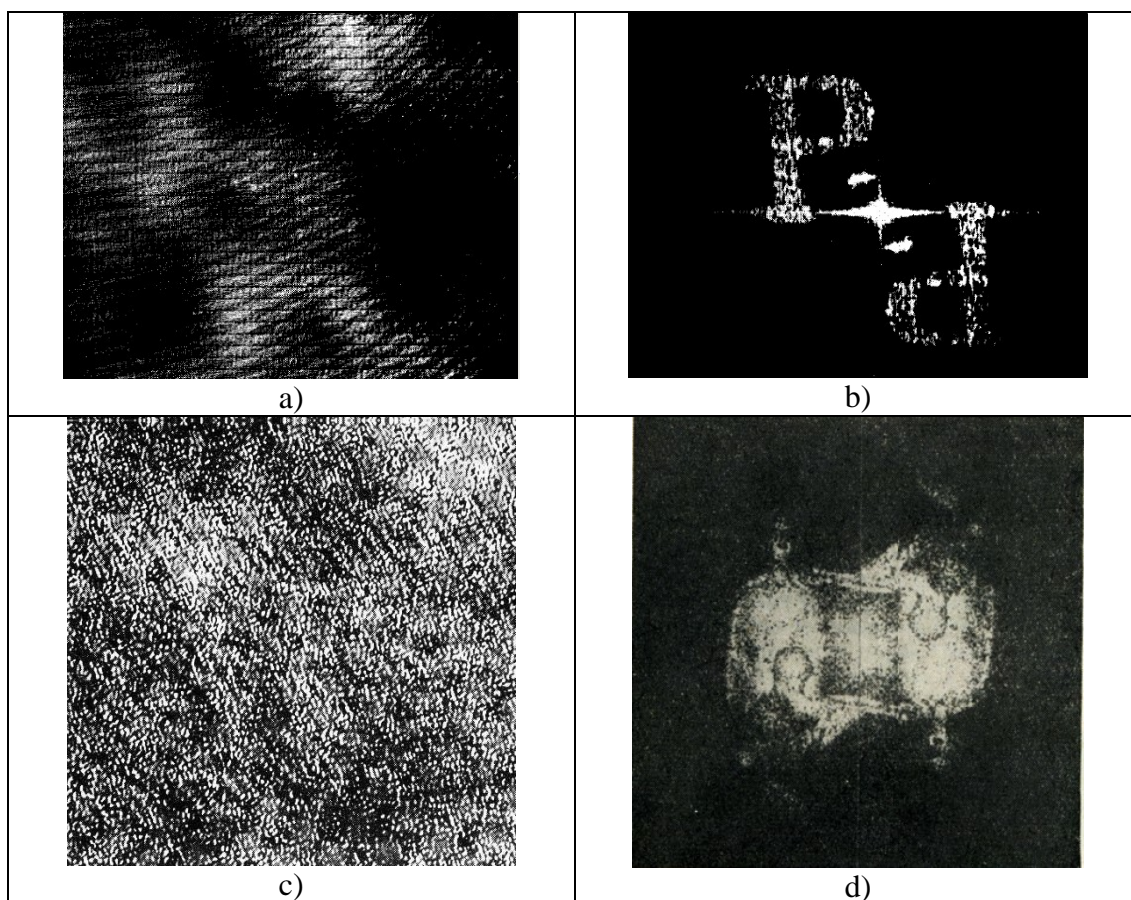


Fig. 3.1 First holograms numerically reconstructed in computers: a) a test optical Fourier hologram electronically recorded using vidicon TV camera to 256x256 pixels quantized to 8 grey levels; b) – image numerically reconstructed from this hologram on a computer PDP-6; c) - a test optical Fourier hologram optically magnified with magnification factor 20, printed and scanned to 512x512 pixels using electro-mechanical scanner with resolution 0.2 mm and quantized to 64 gray levels in a logarithmic scale; d) - two conjugate images reconstructed from this hologram on computer Minsk-22. Images a) and b) are adopted from Ref. 1., images c) and d) are adopted from Ref. 2

Then, with an advent of digital CCD cameras with pitch of 10-20 μm , it had become possible to perform direct digitizing optical hologram in the process of hologram

recording. In first experiments with CCD cameras ([4]), holograms were recorded in the Leith-Upatnieks off axis scheme ([5]). This obviously required at least twice resolution of the camera compared to that defined by the angular size of objects. Later, phase-shifting method of recording holograms was suggested ([6]) that enabled on-axis hologram recording scheme. Since that time, numerous projects in digital recording and numerical reconstruction of optical holograms have been initiated and implemented, especially in the field of optical holographic microscopy. Mathematical models of off-axis and on-axis methods for digital recording of holograms are introduced in Sects. 3.2 and 3.3. In Sect. 3.4, point spread function of numerical reconstruction of holograms are derived. In Sect. 3.5 zones of applicability of Fourier and Convolution algorithms for numerical reconstruction of Fresnel holograms are discussed.

3.2. “Off-axis” digital recording of holograms

Consider a mathematical model of producing and recording holograms. Let $\alpha(f_x, f_y)$ and $R(f_x, f_y)$ denote complex amplitudes of the object and reference beams, respectively, at point (f_x, f_y) of the hologram plane. Then signal recorded by the recording medium at this point is a squared module of their sum:

$$\begin{aligned} H(f_x, f_y) &= |\alpha(f_x, f_y) + R(f_x, f_y)|^2 = \\ &= \alpha(f_x, f_y)R^*(f_x, f_y) + \alpha^*(f_x, f_y)R(f_x, f_y) + |\alpha(f_x, f_y)|^2 + |R(f_x, f_y)|^2, \end{aligned} \quad (3.2.1)$$

where asterisk denotes complex conjugate. This signal is a hologram signal, or a hologram. The first term in the sum in the right hand part of Eq. 3.2.1 is proportional to the object’s beam complex amplitude. This is what we call the mathematical hologram.

Numerical reconstruction of the hologram consists in applying to the mathematical hologram a transform that implements wave back propagation from the hologram plane to object. For this, one has either to eliminate, before the reconstruction, other three terms or to apply the reconstruction transform to the entire hologram and then separate the contribution of other terms in the reconstruction result from that of the mathematical hologram term.

The latter solution is known as a classical Leith-Upatnieks’s method of off-axis recording hologram ([5]). In off-axis recording, a spatial angle between reference and object beams is introduced that exceeds the angular size of the object under which it is seen from the hologram plane (Fig. 3.1).

A drawback of this method is that it requires at least twice as much degrees of freedom (resolution cells) of the recording medium for recording all interference terms described by Eq. 3.1.2 compared to that required for recording only the very first term in Eq. 3.2.1 proportional to the object’s beam complex amplitude.

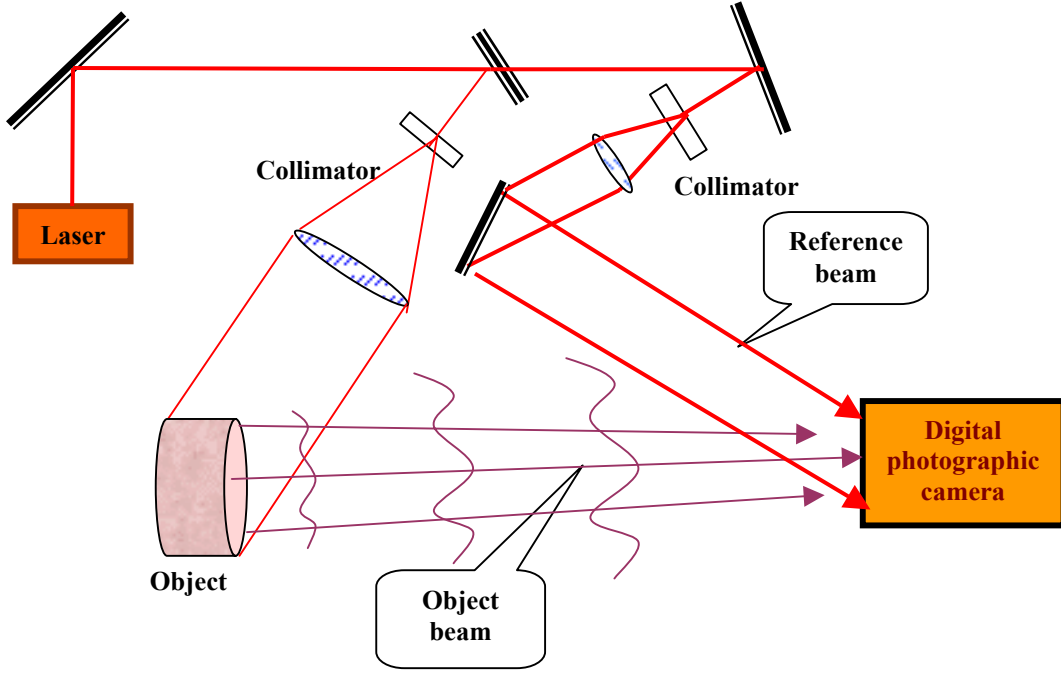


Fig. 3.1. Schematic diagram of “off-axis” method for electronic hologram recording.

3.3. “On-axis” digital recording of holograms

The method of eliminating interfering terms in recorded holograms before the reconstruction is. In the on-axis method of recording holograms, known also as phase-shifting holography ([6]), object and reference beams are co-linear (Fig. 3.2) and several exposures of holograms of the object are carried out with shifting, for each exposure, the phase of the reference beam plane wave front and recording the results of the exposures.

Although the method can, in principle, be implemented for optical recording holograms as well, it was suggested and is used for numerical reconstruction of holograms. In what follows, we show that at least three exposures with phase shifts $2\pi/3$ and $4\pi/3$ with respect to the first one are required in this method.

Let θ_k be a phase shift of the reference beam in k -th hologram exposure, $k = 1, \dots, K$. Then

$$H_k(f_x, f_y) = |\alpha(f_x, f_y) + R(f_x, f_y)\exp(i\theta_k)|^2 = \alpha(f_x, f_y)R^*(f_x, f_y)\exp(-i\theta_k) + \alpha^*(f_x, f_y)R(f_x, f_y)\exp(i\theta_k) + |\alpha(f_x, f_y)|^2 + |R(f_x, f_y)|^2 \quad (3.3.1)$$

is a hologram recorded in k -th exposure. For reconstruction of the term $\alpha(f_x, f_y)$ that represents object wave front, K holograms $\{H_k\}$ are summed up with the same phase shift used in their recording:

$$\bar{H} = \frac{1}{K} \sum_{k=1}^K H_k \exp(i\theta_k) = \alpha(f_x, f_y) R^*(f_x, f_y) + \alpha^*(f_x, f_y) R(f_x, f_y) \sum_{k=1}^K \exp(i2\theta_k) + \left[|\alpha(f_x, f_y)|^2 + |R(f_x, f_y)|^2 \right] \sum_{k=1}^K \exp(i\theta_k). \quad (3.3.2)$$

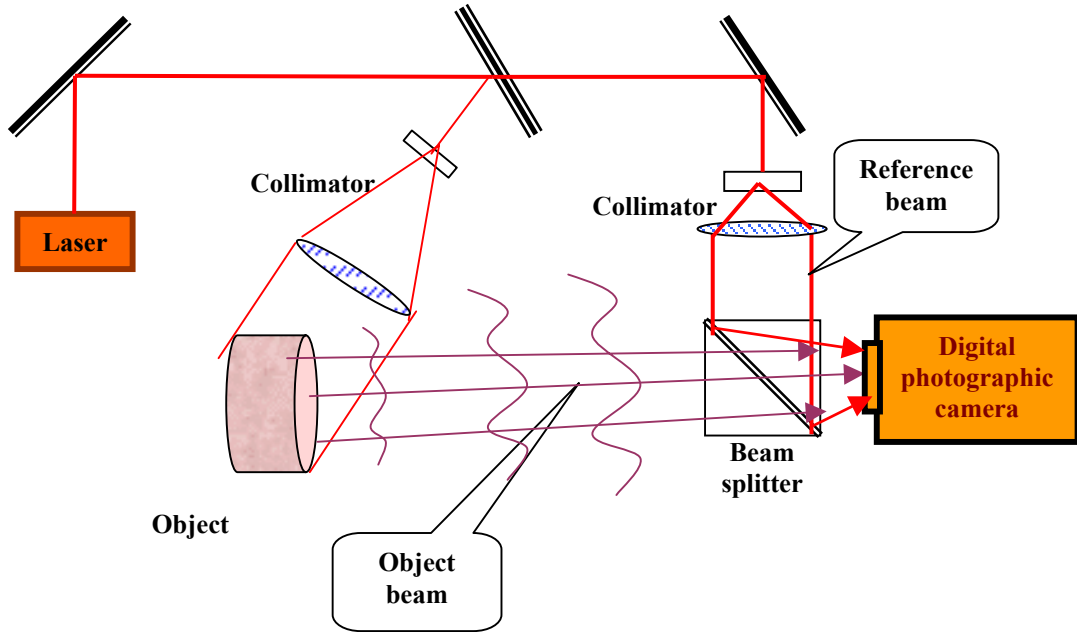


Fig. 3.2. Schematic diagram of “off axis” method for electronic recording of holograms

For perfect reconstruction of the first term, phases $\{\theta_k\}$ should be found from equations:

$$\sum_{k=1}^K \exp(i\theta_k) = 0; \quad (3.3.3, a)$$

$$\sum_{k=1}^K \exp(i2\theta_k) = 0. \quad (3.3.3, b)$$

Assume $\theta_k = k\theta_0$. Then:

$$\begin{aligned} \sum_{k=1}^K \exp(i\theta_k) &= \sum_{k=1}^K \exp(ik\theta_0) = \frac{\exp[i(K+1)\theta_0] - \exp(i\theta_0)}{\exp(i\theta_0) - 1} = \frac{\exp(iK\theta_0) - 1}{\exp(i\theta_0) - 1} \exp(i\theta_0), \\ \sum_{k=1}^K \exp(i2\theta_k) &= \sum_{k=1}^K \exp(i2k\theta_0) = \frac{\exp[i2(K+1)\theta_0] - \exp(i2\theta_0)}{\exp(i2\theta_0) - 1} = \\ &= \frac{\exp(i2K\theta_0) - 1}{\exp(i2\theta_0) - 1} \exp(i2\theta_0) = \frac{\exp(iK\theta_0) - 1}{\exp(i\theta_0) - 1} \frac{\exp(iK\theta_0) + 1}{\exp(i\theta_0) + 1} \exp(i2\theta_0) \end{aligned} \quad (3.3.4)$$

from which it follows that solution of Eq. 3.3.3, a) is $\theta_k = 2\pi \frac{k}{K}$ for any integer $K \geq 3$. For $K = 2$ solution $\theta_0 = \pi$ does not satisfy Eq. 3.3.3, b) as

$$\frac{\exp(i2\theta_0) - 1}{\exp(i\theta_0) - 1} \frac{\exp(i2\theta_0) + 1}{\exp(i\theta_0) + 1} \exp(i2\theta_0) = [\exp(i2\pi) + 1] \exp(i2\pi) = 2. \quad (3.3.5)$$

For example, in four-exposures we will have:
First exposure records:

$$I_1 = \left| U_{ref} \exp(i\varphi_{rref}^{(1)}) + U_{obj} \exp(i\varphi_{obj}) \right|^2 = |U_{ref}|^2 + |U_{obj}|^2 + U_{ref}^* U_{obj} + U_{ref} U_{obj}^*; \quad (3.3.6 a)$$

Second exposure records:

$$I_2 = \left| U_{ref} \exp\left(i\varphi_{rref}^{(1)} + i\frac{\pi}{2}\right) + U_{obj} \exp(i\varphi_{obj}) \right|^2 = |U_{ref}|^2 + |U_{obj}|^2 - iU_{ref}^* U_{obj} + iU_{ref} U_{obj}^*; \quad (3.3.6 b)$$

Third exposure records:

$$I_3 = \left| U_{ref} \exp\left(i\varphi_{rref}^{(1)} + i\pi\right) + U_{obj} \exp(i\varphi_{obj}) \right|^2 = |U_{ref}|^2 + |U_{obj}|^2 - U_{ref}^* U_{obj} - U_{ref} U_{obj}^*; \quad (3.3.6 c)$$

Fourth exposure records:

$$I_4 = \left| U_{ref} \exp\left(i\varphi_{rref}^{(1)} + i\frac{3\pi}{2}\right) + U_{obj} \exp(i\varphi_{obj}) \right|^2 = |U_{ref}|^2 + |U_{obj}|^2 + i\overrightarrow{U_{ref}^*} \overrightarrow{U_{obj}} - i\overrightarrow{U_{ref}} \overrightarrow{U_{obj}^*}. \quad (3.3.6 d)$$

Then the mathematical hologram can be computed as

$$U_{ref}^* U_{obj} = \frac{I_1 + iI_2 - I_3 - iI_4}{4} \quad (3.3.7)$$

3.4. Point spread functions of numerical reconstruction of holograms

3.4.1. A general formulation

In numerical reconstruction of holograms, samples of the object wave front are reconstructed out of samples of its hologram using the discrete diffraction transforms. This process can be treated as object wave front sampling by a sampling system that consists of the hologram sampling device and a computer, in which the object wave front samples are numerically reconstructed from the hologram.

Signal sampling is a linear transformation that is fully specified by its point spread function (PSF), which establishes a link between an object signal $a(x)$ and its samples $\{a_k\}$:

$$a_k = \int_x a(x)PSF(x, k)dx, \quad (3.4.1)$$

According to the sampling theory (see, for instance, [8]), for a given sampling interval Δx , PSF of the ideal sampling device is a sinc-function:

$$PSF(x, k) = \text{sinc}[\pi(x - k\Delta x)/\Delta x] = \frac{\sin[\pi(x - k\Delta x)/\Delta x]}{\pi(x - k\Delta x)/\Delta x} \quad (3.4.2)$$

Provided that the continuous signal is reconstructed from its samples using, as a reconstruction basis functions, the same sinc-functions, this PSF secures minimal root mean square signal reconstruction error.

In this section, we consider point spread functions of different reconstruction algorithms and how do they depend on algorithm parameters and physical parameters of holograms and their sampling devices. For the sake of simplicity, we will consider 1-D holograms and transforms. Corresponding 2-D results are straightforward in the conventional assumption of separability of sampling and transforms.

Let, in numerical reconstruction of holograms, samples $\{a_k\}$ of the object wave front be obtained through a transformation

$$a_k = \sum_{r=0}^{N-1} \alpha_r DRK(r, k). \quad (3.4.3)$$

of available hologram samples $\{\alpha_r\}$ with a certain discrete reconstruction kernel $DRK(r, k)$ that corresponds to the type of the hologram. Hologram samples $\{\alpha_r\}$ are measured by a hologram recording and sampling device as

$$\alpha_r = \int_{-\infty}^{\infty} \alpha(f) \varphi_f^{(s)}(f - \tilde{r}^{(s)} \Delta f^{(s)}) df \quad (3.4.4)$$

where $\alpha(f)$ is a hologram signal, $\{\varphi_f^{(s)}(\cdot)\}$ is a point spread function of the hologram sampling device, $\Delta f^{(s)}$ is a hologram sampling interval, $\tilde{r}^{(s)} = r + \nu^{(s)}$, r is an integer index of hologram samples and $\nu^{(s)}$ is a shift, in units of the hologram

sampling interval, of the hologram sampling grid with respect to the hologram coordinate system.

The hologram signal $\alpha(f)$ is linked with object wave front $a(x)$ through diffraction integral

$$\alpha(f) = \int_{-\infty}^{\infty} a(x) WPK(x, f) dx, \quad (3.4.5)$$

where $WPK(x, f)$ is a wave propagation kernel. Therefore, one can rewrite Eq. 3.3.4 as:

$$\begin{aligned} \alpha_r &= \int_{-\infty}^{\infty} \left[\int_{-\infty}^{\infty} a(x) WPK(x, f) dx \right] \varphi_f^{(s)}(f - \tilde{r}^{(s)} \Delta f^{(s)}) df = \\ &= \int_{-\infty}^{\infty} \int_{-\infty}^{\infty} a(x) WPK(x, f) \varphi_f^{(s)}(f - \tilde{r}^{(s)} \Delta f^{(s)}) dx df = \\ &= \int_{-\infty}^{\infty} a(x) dx \int_{-\infty}^{\infty} WPK(x, f) \varphi_f^{(s)}(f - \tilde{r}^{(s)} \Delta f^{(s)}) df \end{aligned} \quad (3.4.6)$$

Insert now Eq. 3.3.6 into Eq. 3.3.3 and establish a link between object wave front $a(x)$ and its samples $\{a_k\}$ reconstructed from the sampled hologram:

$$\begin{aligned} a_k &= \sum_{r=0}^{N-1} \left[\int_{-\infty}^{\infty} a(x) dx \int_{-\infty}^{\infty} WPK(x, f) \varphi_f^{(s)}(f - \tilde{r}^{(s)} \Delta f^{(s)}) df \right] DRK(r, k) = \\ &= \int_{-\infty}^{\infty} a(x) dx \left[\int_{-\infty}^{\infty} WPK(x, f) df \sum_{r=0}^{N-1} DRK(r, k) \varphi_f^{(s)}(f - \tilde{r}^{(s)} \Delta f^{(s)}) \right] = \int_{-\infty}^{\infty} a(x) PSF(x, k) dx \end{aligned} \quad (3.4.7)$$

where function

$$PSF(x, k) = \int_{-\infty}^{\infty} WPK(x, f) df \sum_{r=0}^{N-1} DRK(r, k) \varphi_f^{(s)}(f - \tilde{r}^{(s)} \Delta f^{(s)}) \quad (3.4.8)$$

can be treated as a *point spread function (PSF) of the numerical reconstruction of holograms*. As one can see from Eq. 7.1.8, it depends on all factors involved in the process of sampling and reconstruction of holograms: wave propagation kernel $WPK(.,.)$, discrete reconstruction kernel $DRK(.,.)$ and point spread function of the hologram sampling device $\varphi_f^{(s)}(.)$.

For further analysis, it is convenient to replace point spread function of the hologram sampling device through its Fourier Transform, or its frequency response $\Phi_f^{(s)}(.)$:

$$\begin{aligned} \varphi_f^{(s)}(f - \tilde{r}^{(s)}\Delta f) = \\ \int_{-\infty}^{\infty} \Phi_f^{(s)}(\xi) \exp[i2\pi(f - \tilde{r}^{(s)}\Delta f^{(s)})\xi] d\xi = \int_{-\infty}^{\infty} \Phi_f^{(s)}(\xi) \exp(-i2\pi\tilde{r}^{(s)}\Delta f^{(s)}\xi) \exp(i2\pi f\xi) d\xi \end{aligned} \quad (3.4.9)$$

Then obtain:

$$\begin{aligned} PSF(x, k) = \int_{-\infty}^{\infty} WPK(x, f) df \sum_{r=0}^{N-1} DRK(r, k) \int_{-\infty}^{\infty} \Phi_f^{(s)}(\xi) \exp(-i2\pi\tilde{r}^{(s)}\Delta f^{(s)}\xi) \exp(i2\pi f\xi) d\xi = \\ \int_{-\infty}^{\infty} \Phi_f^{(s)}(\xi) d\xi \int_{-\infty}^{\infty} WPK(x, f) \exp(i2\pi f\xi) df \sum_{r=0}^{N-1} DRK(r, k) \exp(-i2\pi\tilde{r}^{(s)}\Delta f^{(s)}\xi). \end{aligned} \quad (3.4.10)$$

Introduce function

$$\begin{aligned} \overline{PSF}(x, \xi; k) = \int_{-\infty}^{\infty} WPK(x, f) \exp(i2\pi f\xi) df \sum_{r=0}^{N-1} DRK(r, k) \exp(-i2\pi\tilde{r}^{(s)}\Delta f^{(s)}\xi) = \\ \overline{WPK}(x, \xi) \cdot \overline{DRK}(\xi, k), \end{aligned} \quad (3.4.11)$$

where

$$\overline{WPK}(x, \xi) = \int_{-\infty}^{\infty} WPK(x, f) \exp(i2\pi f\xi) df \quad (3.4.12)$$

is Fourier transform of the wave propagation kernel $WPK(.,.)$ and

$$\overline{DRK}(\xi, k) = \sum_{r=0}^{N-1} DRK(r, k) \exp(-i2\pi\tilde{r}^{(s)}\Delta f^{(s)}\xi), \quad (3.4.13)$$

which is a Fourier series expansion with the discrete reconstruction kernel $DRK(r, k)$ as expansion coefficients.

Function $\overline{PSF}(x, \xi; k)$ does not depend on parameters of the hologram sampling device. We will refer to this function as *PSF of sampled hologram reconstruction*. PSF of the numerical reconstruction of holograms $PSF(x, k)$ and PSF of sampled hologram reconstruction $\overline{PSF}(x, \xi; k)$ are linked through the integral transform

$$PSF(x, k) = \int_{-\infty}^{\infty} \Phi_f^{(s)}(\xi) \overline{PSF}(x, \xi; k) d\xi \quad (3.4.14)$$

with frequency response of the hologram sampling device as a transform kernel.

3.4.2. Point spread function of numerical reconstruction of holograms recorded in far diffraction zone (Fourier holograms)

Consider point spread function of numerical reconstruction of Fourier holograms. For far diffraction zone, wave propagation kernel is that of the integral Fourier transform:

$$WPK(x, f) = \exp\left(-i2\pi \frac{xf}{\lambda Z}\right). \quad (3.4.15)$$

Its Fourier Transform is a delta-function:

$$\begin{aligned} \overline{WPK}(x, \xi) &= \\ \int_{-\infty}^{\infty} WPK(x, f) \exp(i2\pi f \xi) df &= \int_{-\infty}^{\infty} \exp\left[-i2\pi f \left(\frac{x}{\lambda Z} - \xi\right)\right] df = \delta\left(\frac{x}{\lambda Z} - \xi\right). \end{aligned} \quad (3.4.16)$$

Assume that Shifted DFT with discrete reconstruction kernel

$$DRK(r, k) = \exp\left[i2\pi \frac{(k+u)(r+v)}{N}\right]. \quad (3.4.16)$$

is used for numerical reconstruction of Fourier hologram. Fourier series expansion over this discrete reconstruction kernel is:

$$\begin{aligned} \overline{DRK}(\xi, k) &= \sum_{r=0}^{N-1} DRK(r, k) \exp(-i2\pi \tilde{v}^{(s)} \Delta f^{(s)} \xi) = \\ \sum_{r=0}^{N-1} \exp\left[i2\pi \frac{(k+u)(r+v)}{N}\right] \exp[-i2\pi (r+v^{(s)}) \Delta f^{(s)} \xi] &= \\ \exp(-i2\pi v^{(s)} \Delta f^{(s)} \xi) \exp\left[i2\pi \frac{(k+u)v}{N}\right] \sum_{r=0}^{N-1} \exp\left[i2\pi \left(\frac{(k+u)}{N} - \Delta f^{(s)} \xi\right) r\right] &= \\ \exp(-i2\pi v^{(s)} \Delta f^{(s)} \xi) \exp\left[i2\pi \frac{(k+u)v}{N}\right] \frac{\exp\left[i2\pi N \left(\frac{(k+u)}{N} - \Delta f^{(s)} \xi\right)\right]^{-1}}{\exp\left[i2\pi \left(\frac{(k+u)}{N} - \Delta f^{(s)} \xi\right)\right]^{-1}} &= \\ \exp\left[-i2\pi \left(v^{(s)} + \frac{N-1}{2}\right) \Delta f^{(s)} \xi\right] \exp\left\{i2\pi \frac{(k+u)}{N} \left(v + \frac{N-1}{2}\right)\right\} \times \\ \frac{\sin\left[\pi N \left(\Delta f^{(s)} \xi - \frac{k+u}{N}\right)\right]}{\sin\left[\pi \left(\Delta f^{(s)} \xi - \frac{k+u}{N}\right)\right]} & \end{aligned} \quad (3.4.17)$$

It is only natural now to choose shift parameters $\nu^{(s)}$ and ν of sampling and reconstruction transform as:

$$\nu^{(s)} = \nu = -\frac{N-1}{2}. \quad (3.4.18)$$

With these shift parameters,

$$\overline{DRK}(\xi, k) = \frac{\sin\left[\pi\left(\Delta f^{(s)}\xi - \frac{(k+u)}{N}\right)N\right]}{\sin\left[\pi\left(\Delta f^{(s)}\xi - \frac{(k+u)}{N}\right)\right]} = N \operatorname{sincd}\left[N; \pi\left(\Delta f^{(s)}\xi - \frac{(k+u)}{N}\right)N\right] \quad (3.4.19)$$

and

$$\begin{aligned} \overline{PSF}(x, \xi; k) &= \overline{WPK}(x, \xi) \cdot \overline{DRK}(\xi, k) \\ N \operatorname{sincd}\left[N; \pi\left(\Delta f^{(s)}\xi - \frac{(k+u)}{N}\right)N\right] &\delta\left(\frac{x}{\lambda Z} - \xi\right). \end{aligned} \quad (3.4.20)$$

Then, finally, obtain that the point spread function of numerical reconstruction of Fourier hologram is

$$\begin{aligned} PSF(x, k) &= \int_{-\infty}^{\infty} \Phi_f^{(s)}(\xi) \overline{PSF}(x, \xi; k) d\xi = \\ N \operatorname{sincd}\left[N; \pi\left(\frac{\Delta f^{(s)}x}{\lambda Z} - \frac{(k+u)}{N}\right)N\right] &\int_{-\infty}^{\infty} \Phi_f^{(s)}(\xi) \delta\left(\frac{x}{\lambda Z} - \xi\right) d\xi \\ = N \operatorname{sincd}\left[N; \pi\left(\frac{\Delta f^{(s)}x}{\lambda Z} - \frac{(k+u)}{N}\right)N\right] &\Phi_f^{(s)}\left(\frac{x}{\lambda Z}\right) = \\ = N \operatorname{sincd}\left[N; \pi(x - (k+u)\Delta_x)/\Delta_x\right] &\Phi_f^{(s)}\left(\frac{x}{\lambda Z}\right), \end{aligned} \quad (3.4.21)$$

where

$$\Delta_x = \lambda Z / N \Delta f^{(s)} = \lambda Z / S_H \quad (3.4.22)$$

and $S_H = N \Delta f^{(s)}$ is the physical size of the hologram.

Formula (3.4.21) has a clear physical interpretation illustrated in Fig.3.3. As it was mentioned, point spread function of the ideal signal sampling device is a sinc-function and its frequency response is a rect-function. Provided the hologram sampling device is such an ideal sampler with frequency response:

$$\Phi_f^{(s)}\left(\frac{x}{\lambda Z}\right) = \operatorname{rect}\left(\frac{x + \lambda Z / 2 \Delta f^{(s)}}{\Delta f^{(s)} / \lambda Z}\right) = \begin{cases} 1, & -\lambda Z / 2 \Delta f^{(s)} \leq x \leq \lambda Z / 2 \Delta f^{(s)} \\ 0, & \text{otherwise} \end{cases}, \quad (3.4.23)$$

point spread function of numerical reconstruction of Fourier hologram is a discrete sinc-function, and object wave front samples are measured within the object's spatial extent interval $-\lambda Z / 2 \Delta f^{(s)} \leq x \leq \lambda Z / 2 \Delta f^{(s)}$ defined by the spread of the hologram

sampling device frequency response. Therefore, with an ideal hologram sampler, numerical reconstruction of Fourier hologram is almost ideal object wave front sampling, as discrete sinc-function approximates continuous sinc-function within the interval $-\lambda Z/2\Delta f^{(s)} \leq x \leq \lambda Z/2\Delta f^{(s)}$ relatively closely, the closer, the larger is the number of hologram samples N . Parameter Δ_x defined by Eq. 3.4.22 is half width of the main lobe of the discrete sinc-function. It characterizes the virtual inter-sample distance and the resolving power of the reconstruction algorithm.

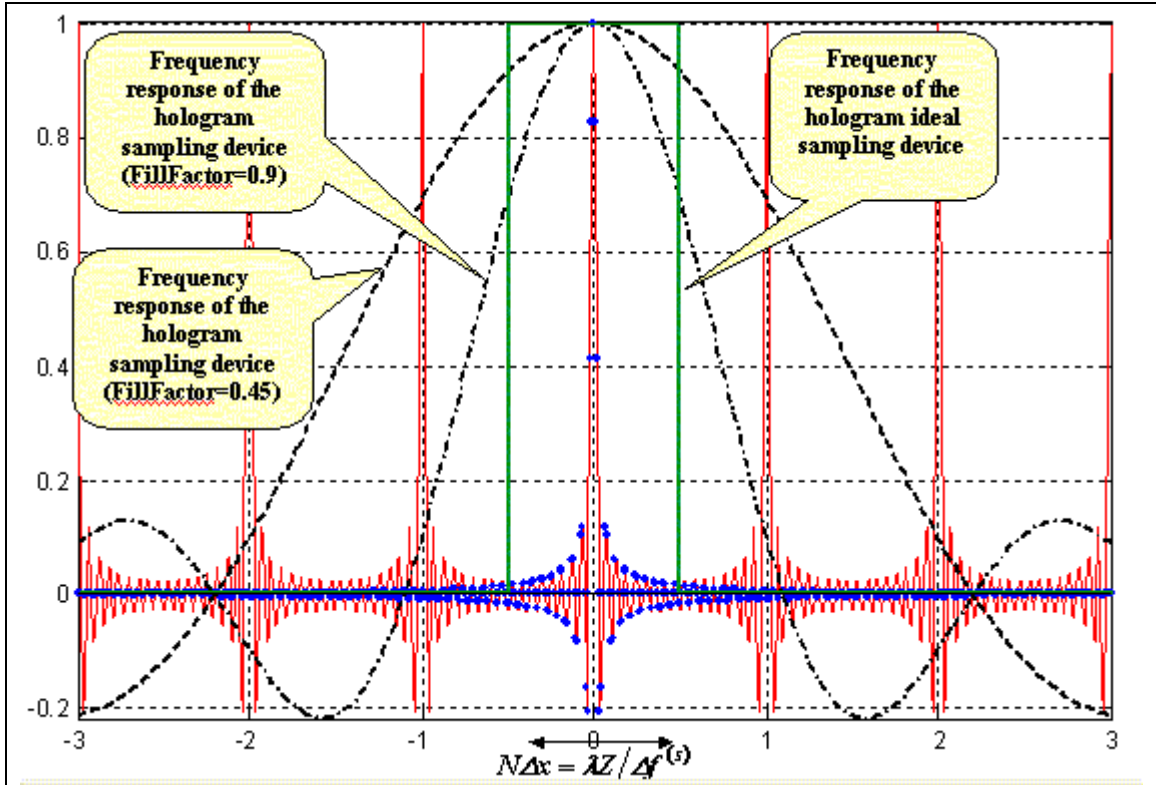


Fig. 3.3. PSF of numerical reconstruction of holograms digitally recorded in far diffraction zone (thin solid line). Rectangle in bold line is Fourier Transform of the hologram ideal sampling device. Bold dots plot sinc-function, the ideal sampling PSF.

In reality, hologram sampling devices are, of course, not ideal samplers, and their frequency responses are not rectangular functions. They are not uniform within the basic object extend interval $-\lambda Z/2\Delta f^{(s)} \leq x \leq \lambda Z/2\Delta f^{(s)}$ and decay not abruptly outside this interval but rather gradually. As a consequence, each of the object samples is a combination of the sample, measured by the main lobe of the discrete sinc-function within the basic object extend interval and samples collected by other lobes of the discrete sinc-function outside the basic interval. This is one source of the measurement errors. In particular, for diffusely reflecting objects, it may result in an additional speckle noise in the reconstructed object image. One can avoid this distortion if, in the process of making object hologram, object is illuminated strictly within the basic interval as defined by the hologram sampling interval (camera pitch).

The second source of the reconstruction errors is associated with non-uniformity of the hologram sampler frequency response within the basic interval. These errors can be compensated by multiplying the reconstruction results by the function inverse to the frequency response of the hologram sampler.

One can also see from Eq. 3.4.21 that the resolving power of numerical reconstruction of Fourier hologram is determined by the distance between zeros of the discrete sinc-function, which is equal to $\lambda Z / N \Delta f^{(s)} = \lambda Z / S_H$, where $S_H = N \Delta f^{(s)}$ is size of the sampled hologram. Due to this finite resolving power, one can also expect, for diffuse objects, a certain amount of speckle noise in the reconstructed object.

3.4.3. Point spread function of numerical reconstruction of holograms recorded in near diffraction zone (Fresnel holograms)

For near diffraction zone wave propagation kernel is

$$WPK(x, f) \propto \exp\left[i\pi \frac{(x-f)^2}{\lambda Z}\right]. \quad (3.4.24)$$

Its Fourier Transform is:

$$\begin{aligned} \overline{WPK}(x, \xi) &\propto \int_{-\infty}^{\infty} \exp\left[i\pi \frac{(x-f)^2}{\lambda Z}\right] \exp(i2\pi f \xi) df = \\ &\exp(i2\pi x \xi) \int_{-\infty}^{\infty} \exp\left(i\pi \frac{f^2}{\lambda Z}\right) \exp(i2\pi f \xi) df, \end{aligned} \quad (3.4.25)$$

or, with an account of Eq. A.2.1.1 (Appendix A2.1, Lect. 2),

$$\overline{WPK}(x, \xi) \propto \exp(i2\pi x \xi) \exp(-i\pi \lambda Z \xi^2) \quad (3.4.26)$$

In what follows, we will separately consider point spread function for Fourier and Convolution reconstruction algorithms. For simplicity, zero shifts will be assumed in both, hologram and object wave front domains

Fourier reconstruction algorithm

In the Fourier reconstruction algorithm, discrete reconstruction kernel is, with zero shifts in hologram and object wave front domains,

$$DRK(r, k) = \left[\exp\left(-i\pi \frac{k^2 \mu^2}{N}\right) \exp\left(i2\pi \frac{kr}{N}\right) \right] \exp\left(-i\pi \frac{r^2}{\mu^2 N}\right). \quad (3.4.27)$$

Fourier series expansion over this kernel is

$$\begin{aligned} \overline{DRK}(\xi, k) &= \exp\left(-i\pi \frac{k^2 \mu^2}{N}\right) \sum_{r=0}^{N-1} \exp\left(-i\pi \frac{r^2}{\mu^2 N}\right) \exp\left(i2\pi \frac{kr}{N}\right) \exp(-i2\pi r \Delta f^{(s)} \xi) = \\ &\exp\left(-i\pi \frac{k^2 \mu^2}{N}\right) \sum_{r=0}^{N-1} \exp\left(-i\pi \frac{r^2}{\mu^2 N}\right) \exp\left[i2\pi r \left(\frac{k}{N} - \Delta f^{(s)} \xi\right)\right], \end{aligned} \quad (3.4.28, a)$$

or, in a more compact form,

$$\overline{DRK}(\xi, k) = \exp\left(-i\pi \frac{k^2 \mu^2}{N}\right) \text{frinced}\left(N; -1/\mu^2; \frac{k}{N} - \Delta f^{(s)} \xi\right). \quad (3.4.28, b)$$

Then obtain that PSF of sampled hologram reconstruction is

$$\overline{PSF}(x, \xi; k) = \overline{WPK}(x, \xi) \cdot \overline{DRK}(\xi, k) \propto \exp(i2\pi x \xi) \exp(-i\pi \lambda Z \xi^2) \exp\left(-i\pi \frac{k^2 \mu^2}{N}\right) \text{frincd}\left(N; -1/\mu^2; \frac{k}{N} - \Delta f^{(s)} \xi\right) \quad (3.4.29)$$

and that PSF of numerical reconstruction of Fresnel holograms with Fourier reconstruction algorithm is:

$$PSF(x, k) = \exp\left(-i\pi \frac{k^2 \mu^2}{N}\right) \times \int_{-\infty}^{\infty} \Phi_f^{(s)}(\xi) \exp(-i\pi \lambda Z \xi^2) \text{frincd}^*\left(N; 1/\mu^2; \frac{k}{N} - \Delta f^{(s)} \xi\right) \exp(i2\pi x \xi) d\xi \quad (3.4.30)$$

Eqs. 3.4.30 is much more involved for an analytical treatment than the corresponding equation for PSF of numerical reconstruction of Fourier holograms and, in general, requires numerical methods for analysis. In order to facilitate its treatment, rewrite Eq. 3.4.30 using Eq. 3.4.28, a) for $\overline{DRK}(\xi, k)$:

$$\begin{aligned} PSF(x, k) &= \exp\left[i\pi \left(\frac{x^2}{\lambda Z} - \frac{k^2 \mu^2}{N}\right)\right] \times \\ &\int_{-\infty}^{\infty} \Phi_f^{(s)}(\xi) \sum_{r=0}^{N-1} \exp\left(-i\pi \frac{r^2}{\mu^2 N}\right) \exp\left[i2\pi r \left(\frac{k}{N} - \Delta f^{(s)} \xi\right)\right] \exp\left[-i\pi \frac{(x - \lambda Z \xi)^2}{\lambda Z}\right] d\xi = \\ &\exp\left[i\pi \left(\frac{x^2}{\lambda Z} - \frac{k^2 \mu^2}{N}\right)\right] \sum_{r=0}^{N-1} \exp\left(-i\pi \frac{r^2}{\mu^2 N}\right) \exp\left(i2\pi \frac{kr}{N}\right) \times \\ &\int_{-\infty}^{\infty} \Phi_f^{(s)}(\xi) \exp\left[-i\pi \frac{(x - \lambda Z \xi)^2}{\lambda Z}\right] \exp(-i2\pi r \Delta f^{(s)} \xi) d\xi \end{aligned} \quad (3.4.31)$$

Assume now that frequency response of the hologram sampling device $\Phi_f^{(s)}(\xi)$ is constant, which is equivalent to the assumption that its PSF is a delta function. Practically, this means that the hologram recording photographic camera is assumed to have a very small fill-factor, or the ratio of the size of camera sensitive elements to the inter-pixel distance. In this simplifying assumption,

$$\begin{aligned} PSF_0(x, k) &= \exp\left[i\pi \left(\frac{x^2}{\lambda Z} - \frac{k^2 \mu^2}{N}\right)\right] \times \\ &\sum_{r=0}^{N-1} \exp\left(-i\pi \frac{r^2}{\mu^2 N}\right) \exp\left(i2\pi \frac{kr}{N}\right) \int_{-\infty}^{\infty} \exp\left[-i\pi \frac{(x - \lambda Z \xi)^2}{\lambda Z}\right] \exp(-i2\pi r \Delta f^{(s)} \xi) d\xi = \\ &\exp\left[i\pi \left(\frac{x^2}{\lambda Z} - \frac{k^2 \mu^2}{N}\right)\right] \times \end{aligned}$$

$$\begin{aligned}
& \sum_{r=0}^{N-1} \exp\left(-i\pi \frac{r^2}{\mu^2 N}\right) \exp\left(i2\pi \frac{kr}{N}\right) \int_{-\infty}^{\infty} \exp\left[-i\pi \frac{(x-\lambda Z \xi)^2}{\lambda Z}\right] \exp(-i2\pi r \Delta f^{(s)} \xi) d\xi = \\
& \exp\left[i\pi \left(\frac{x^2}{\lambda Z} - \frac{k^2 \mu^2}{N}\right)\right] \times \\
& \sum_{r=0}^{N-1} \exp\left(-i\pi \frac{r^2}{\mu^2 N}\right) \exp\left(i2\pi \frac{kr}{N}\right) \int_{-\infty}^{\infty} \exp\left(-i\pi \frac{\tilde{\xi}^2}{\lambda Z}\right) \exp\left(-i2\pi r \Delta f^{(s)} \frac{x-\tilde{\xi}}{\lambda Z}\right) d\tilde{\xi} = \\
& \exp\left[i\pi \left(\frac{x^2}{\lambda Z} - \frac{k^2 \mu^2}{N}\right)\right] \times \sum_{r=0}^{N-1} \exp\left(-i\pi \frac{r^2}{\mu^2 N}\right) \exp\left(i2\pi \frac{kr}{N}\right) \exp\left(-i2\pi r \Delta f^{(s)} \frac{x}{\lambda Z}\right) \times \\
& \int_{-\infty}^{\infty} \exp\left(-i\pi \frac{\tilde{\xi}^2}{\lambda Z}\right) \exp\left(i2\pi \frac{r \Delta f^{(s)}}{\lambda Z} \tilde{\xi}\right) d\tilde{\xi} \propto \exp\left[i\pi \left(\frac{x^2}{\lambda Z} - \frac{k^2 \mu^2}{N}\right)\right] \times \\
& \sum_{r=0}^{N-1} \exp\left(-i\pi \frac{r^2}{\mu^2 N}\right) \exp\left[i2\pi \left(\frac{k}{N} - \frac{\Delta f^{(s)} x}{\lambda Z}\right) r\right] \exp\left(i\pi \frac{r^2 \Delta f^{(s)2}}{\lambda Z}\right) = \\
& \exp\left[i\pi \left(\frac{x^2}{\lambda Z} - \frac{k^2 \mu^2}{N}\right)\right] \sum_{r=0}^{N-1} \exp\left[-i\pi \left(\frac{N \Delta f^{(s)2}}{\lambda Z} - \frac{1}{\mu^2}\right) \frac{r^2}{N}\right] \exp\left[i2\pi \left(\frac{k}{N} - \frac{\Delta f^{(s)} x}{\lambda Z}\right) r\right],
\end{aligned} \tag{3.4.32 a}$$

or

$$PSF_0(x, k) = \exp\left[i\pi \left(\frac{x^2}{\lambda Z} - \frac{k^2 \mu^2}{N}\right)\right] \text{frincd}^* \left(N; \frac{N \Delta f^{(s)2}}{\lambda Z} - \frac{1}{\mu^2}; \frac{k}{N} - \frac{\Delta f^{(s)} x}{\lambda Z} \right). \tag{3.4.32, b}$$

As one can see from Eq. 3.3.3.9, b), PSF of numerical reconstruction of Fresnel holograms recorded with cameras with very small fill-factor is basically proportional to frincd-function illustrated in Figs. 2.3 and 2,4 (Lect. 2).

An important special case is “in focus” reconstruction, when

$$\mu^2 = \frac{\lambda Z}{N \Delta f^{(s)2}} \tag{3.4.33}$$

In this case numerical reconstruction point spread function is discrete sinc-function

$$\begin{aligned}
PSF_0(x, k) &= \exp\left[i \frac{\lambda Z}{\Delta f^{(s)2}} \left(\frac{\Delta f^{(s)2} x^2}{\lambda^2 Z^2} - \frac{k^2}{N^2}\right)\right] \text{sincd}\left[N; \pi \left(\frac{\Delta f^{(s)} x}{\lambda Z} - \frac{k}{N}\right) N\right] = \\
& \exp\left[i \frac{\lambda Z}{\Delta f^{(s)2}} \left(\frac{\Delta f^{(s)2} x^2}{\lambda^2 Z^2} - \frac{k^2}{N^2}\right)\right] \text{sincd}[N; \pi(x - k \Delta_x) / \Delta_x]
\end{aligned} \tag{3.4.34}$$

where $\Delta_x = \lambda Z / N \Delta f^{(s)} = \lambda Z / S_H$. As one can see, “in focus” reconstruction PSF is essentially the same as that of numerical reconstruction of Fourier holograms (Eq. (3.4.22) for the same assumption regarding the hologram sampling device. It has the

same resolving power and provides aliasing free object reconstruction within the interval $S_o = \lambda Z / \Delta f^{(s)}$.

One can establish a link between the size of this interval and the value $\mu^2 = \lambda Z / N \Delta f^{(s)^2} = \lambda Z N / S_H^2$ of the focusing parameter required for the reconstruction:

$$S_o = \lambda Z / \Delta f^{(s)} = \lambda Z N / S_H = \mu^2 S_H \quad (3.4.35)$$

From this relationship it follows that aliasing free reconstruction of the object from a hologram recorded on a distance defined by the focusing parameter μ^2 is possible if the object size does not exceed the value $\mu^2 S_H$. Therefore, for $\mu^2 < 1$, allowed object size should be less then the hologram size otherwise aliasing caused by the periodicity of the discrete sinc-function will appear.

Convolution reconstruction algorithm

In the convolution reconstruction algorithm, discrete reconstruction kernel is, with zero shifts in hologram and object wave front domains,

$$DRK(r, k) = \text{frincd}(N; \mu^2; k - r) = \frac{1}{N} \sum_{s=0}^{N-1} \exp\left(i\pi \frac{\mu^2 s^2}{N}\right) \exp\left[-i2\pi \frac{(k-r)s}{N}\right] \quad (3.4.36)$$

Fourier series expansion over this kernel is

$$\begin{aligned} \overline{DRK}(\xi, k) &= \frac{1}{N} \sum_{r=0}^{N-1} \sum_{s=0}^{N-1} \exp\left(i\pi \frac{\mu^2 s^2}{N}\right) \exp\left[-i2\pi \frac{(k-r)s}{N}\right] \exp(-i2\pi r \Delta f^{(s)} \xi) = \\ &= \frac{1}{N} \sum_{s=0}^{N-1} \exp\left(i\pi \frac{\mu^2 s^2}{N}\right) \exp\left(-i2\pi \frac{ks}{N}\right) \sum_{r=0}^{N-1} \exp\left[i2\pi r \left(\frac{s}{N} - \Delta f^{(s)} \xi\right)\right]. \end{aligned} \quad (3.4.37)$$

Then obtain that PSF of sampled hologram reconstruction is

$$\begin{aligned} \overline{PSF}(x, \xi; k) &= \overline{WPK}(x, \xi) \cdot \overline{DRK}(\xi, k) \propto \frac{\exp(i2\pi x \xi) \exp(-i\pi \lambda Z \xi^2)}{N} \times \\ &= \sum_{s=0}^{N-1} \exp\left(i\pi \frac{\mu^2 s^2}{N}\right) \exp\left(-i2\pi \frac{ks}{N}\right) \sum_{r=0}^{N-1} \exp\left[i2\pi r \left(\frac{s}{N} - \Delta f^{(s)} \xi\right)\right] \end{aligned} \quad (3.4.38)$$

and that PSF of numerical reconstruction of Fresnel holograms with Fourier reconstruction algorithm is:

$$\begin{aligned} PSF(x, k) &= \int_{-\infty}^{\infty} \Phi_f^{(s)}(\xi) \exp(-i\pi \lambda Z \xi^2) \exp(i2\pi x \xi) d\xi \times \\ &= \frac{1}{N} \sum_{s=0}^{N-1} \exp\left(i\pi \frac{\mu^2 s^2}{N}\right) \exp\left(-i2\pi \frac{ks}{N}\right) \sum_{r=0}^{N-1} \exp\left[i2\pi r \left(\frac{s}{N} - \Delta f^{(s)} \xi\right)\right] = \end{aligned}$$

$$\int_{-\infty}^{\infty} \Phi_f^{(s)}(\xi) \exp(-i\pi\lambda Z \xi^2) \exp(i2\pi x \xi) d\xi \sum_{s=0}^{N-1} \exp\left(i\pi \frac{\mu^2 s^2}{N}\right) \exp\left(-i2\pi \frac{ks}{N}\right) \times \frac{\sin\left[\pi\left(s - N\Delta f^{(s)}\xi\right)\right]}{N \sin\left[\frac{\pi}{N}\left(s - N\Delta f^{(s)}\xi\right)\right]} \exp\left[i\pi \frac{N-1}{N}\left(s - N\Delta f^{(s)}\xi\right)\right], \quad (3.4.39)$$

or finally,

$$PSF(x, k) = \int_{-\infty}^{\infty} \Phi_f^{(s)}(\xi) \exp(-i\pi\lambda Z \xi^2) \exp(i2\pi x \xi) d\xi \sum_{s=0}^{N-1} \exp\left(i\pi \frac{\mu^2 s^2}{N}\right) \exp\left(-i2\pi \frac{ks}{N}\right) \times \text{sincd}\left[N; \pi\left(s - N\Delta f^{(s)}\xi\right)\right] \exp\left[i\pi \frac{N-1}{N}\left(s - N\Delta f^{(s)}\xi\right)\right] \quad (3.4.40)$$

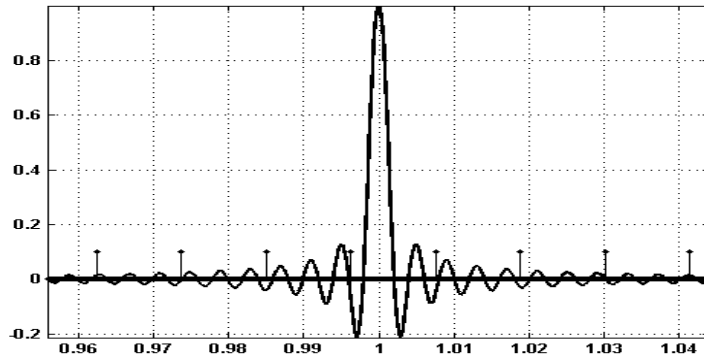
Note that the last phase exponential term in Eq. 3.4.40 is inessential, as it appears due to the assumption of zero shift parameters in the reconstruction algorithm.

Although Eq. 3. 3.4.40 is quite nontransparent for analysis, at least one important property, that of periodicity of the PSF over object sample index k with period N , can be immediately seen from it. As, by the definition of the Convolutional Fresnel Transform, sampling interval $\Delta \mathbf{x}^{(r)}$ in the object plane is identical to the hologram sampling interval $\Delta \mathbf{f}^{(s)}$, this periodicity of the PSF implies that object wave front is reconstructed within the physical interval $N\Delta \mathbf{x} = N\Delta \mathbf{f}^{(s)} = \mathbf{S}_H$, where \mathbf{S}_H is the physical size of the hologram. Further detailed analysis is not feasible without bringing in numerical methods. Some results of such a numerical analysis¹ are illustrated in Fig. 3.4.

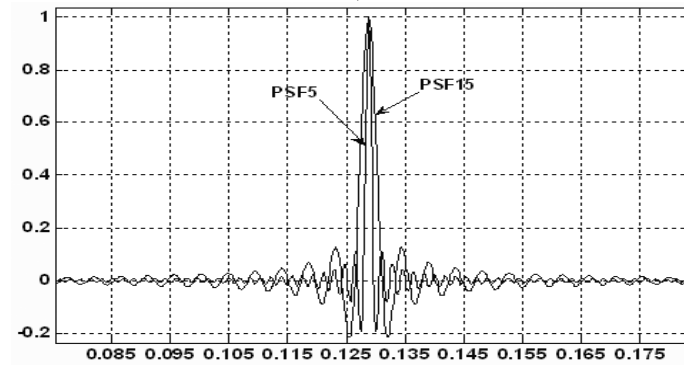
Figs. 3.4, a) and b), in particular, reveal that, although object sampling interval in the convolution method is deliberately set equal to the hologram sampling interval, resolving power of the method is still defined by the same fundamental value $\lambda Z / \mathbf{S}_H$ as that of the Fourier reconstruction algorithm and of the Fourier reconstruction algorithm for Fourier holograms. One can clearly see this when one compares width of the main lobe of the point spread function in Fig. 3.4, a) with the distance between vertical ticks that indicate object sampling positions and from observing, in Fig. 3.4, b), three times widening of the width of the main lobe of PSF that corresponds to the object-to-hologram distance $Z = 15$ with respect to that for $Z = 5$. Fig. 3.4, c) shows reconstruction of nine point sources placed uniformly within the object size. The plot vividly demonstrates that the hologram sampling device point function acts very similarly to its action in case of the Fourier reconstruction algorithm and of reconstruction of Fourier holograms: it is masking the reconstruction result with a function close to its Fourier transform.

Finite width of the reconstruction algorithm PSFs does not only limits their resolving power. It also causes speckle noise in the reconstruction of diffuse objects. This phenomenon is illustrated in Fig. 3.5 that compares reconstructions of rectangular shaped non-diffuse and diffuse objects.

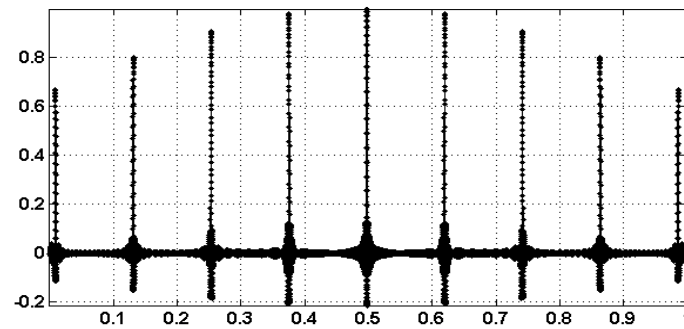
¹ The analysis was carried out with the help of Dr. Fucai Zhang, Institute of Technical Optics, Stuttgart University, Germany



a)



b)



c)

Fig. 3.4. Point spread function of the convolution algorithm: a) – central lobe of the PSF shown along with boundaries of object sampling interval (vertical ticks); b) PSF of reconstructions for two distances between object and hologram ($Z=5$ and $Z=15$); c) reconstruction result for 9 point sources placed uniformly within object area.

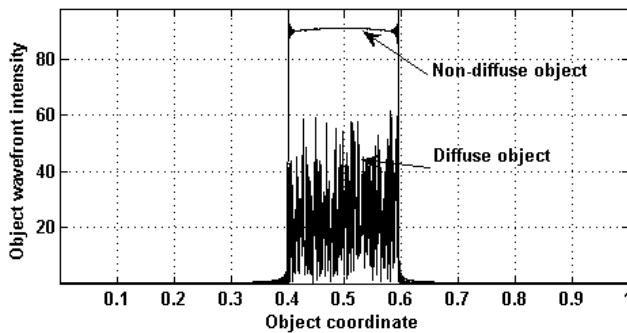


Fig. 3.5. Results of computer simulation reconstruction by the convolution algorithm of a Fresnel hologram of non-diffuse and diffuse objects that demonstrate appearance of heavy speckle noise for the diffuse object.

3.5. Zones of applicability of the Fourier and convolution reconstruction algorithms

From the above analysis of point spread functions of the Fourier and Convolution algorithms, as well as from properties of the fringed-function outlined in Lect.2 it follows that the algorithms has different zones of application in terms of the distance parameter $\mu^2 = \lambda Z / N \Delta f^{(s)2} = \lambda Z N / S_H^2$ that connects wave length of the object illumination λ , distance between the object and hologram planes Z , the number of hologram samples N , pitch of the hologram recording camera $\Delta f^{(s)2}$ and its size S_H (for the fringed-function the corresponding parameter is $q = 1/\mu^2$). Specifically, Fourier reconstruction algorithm provides aliasing-free reconstruction for distances that are large enough to secure that $\mu^2 \geq 1$ ($q \leq 1$) while the convolution algorithm works aliasing-free reconstruction for closer distances when $\mu^2 \leq 1$ ($q \geq 1$). When $\mu^2 = 1$ ($q = 1$) both methods give identical results. These two zones are sketched in Fig. 3.6.

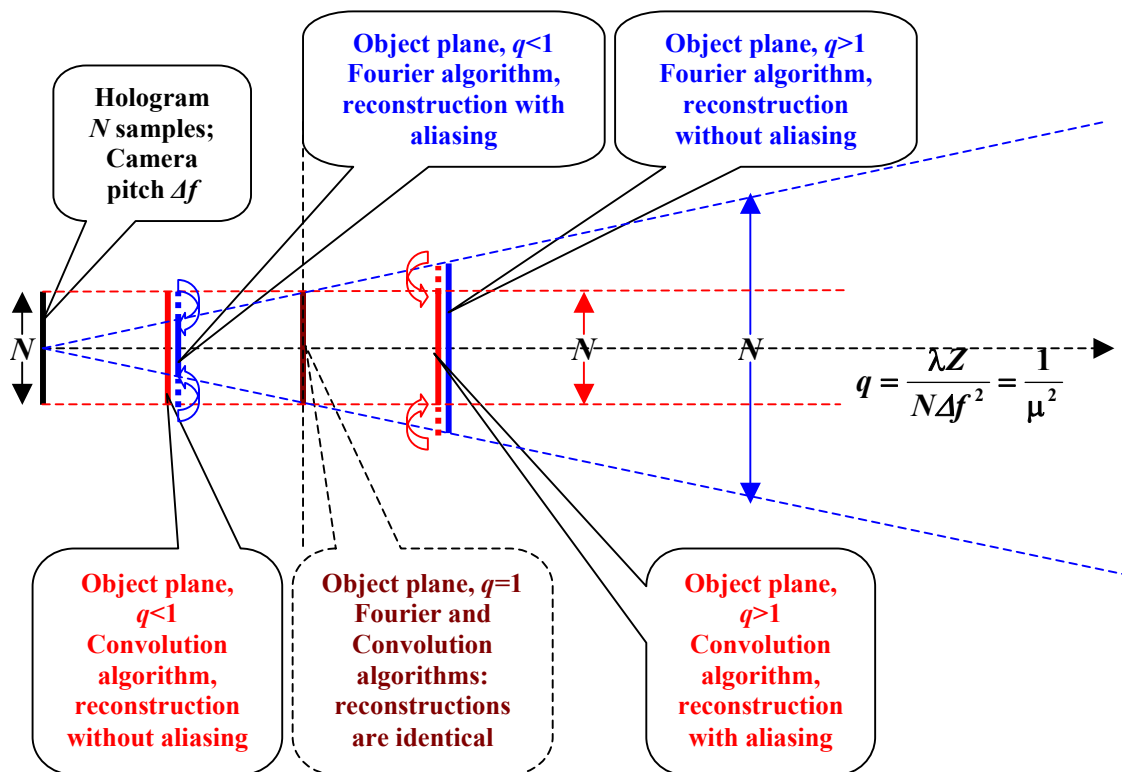


Fig. 3.6. Zones of applicability of Fourier and Convolution algorithms for numerical reconstruction of Fresnel holograms.

This phenomena of aliasing are illustrated in movie shown in Fig. 3.7, a) that shows results of reconstruction of a Fresnel hologram of test object sketched in Fig. 3.7, b) that consists of two crossed thin wires and a ruler installed at different distances from the hologram².

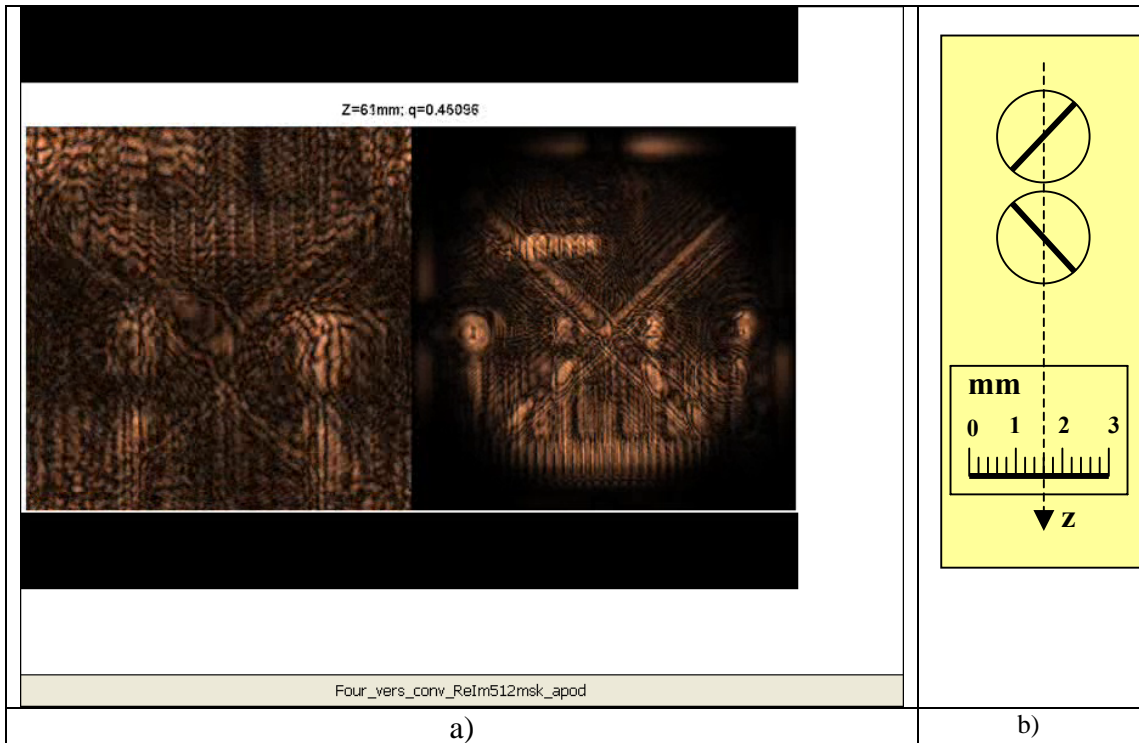


Fig. 3.7. A movie (a) illustrating reconstruction of a Fresnel hologram of a test object (b) by means of Fourier (left) and Convolution (right) algorithms.

Fig. 3.8 shows several particular frames of this movie obtained for focusing parameter $\mu^2 = 0.2439$, $\mu^2 = 0.6618$ and $\mu^2 = 1$. One can clearly see in Fig. 3.8, aliasing artifacts in the Fourier reconstruction due to overlapping of reconstructions from two side lobes of the discrete sinc-functions for $\mu^2 = 0.2439$, $\mu^2 = 0.6618$. One can remove these artifacts if, before the reconstruction, sets to zeros outer parts of the hologram outside the circle with diameter equal to μ^2 -th fraction of the hologram size. The result of such a reconstruction is shown in Fig. 3.8, middle column. Note that Fourier reconstruction algorithm with above mentioned zeroing of the excessive part of the hologram, acts for $\mu^2 < 1$, with respect to the convolution algorithm reconstruction as a “magnifying glass”. Object aliasing artifacts of the Fourier reconstruction algorithm for $\mu^2 < 1$ can also be avoided if the hologram is reconstructed by fragments of $\mu^2 S_H$ size.

² The hologram courtesy to Dr. J. Campos, Autonomous University of Barcelona, Bellaterra, Barcelona, Spain

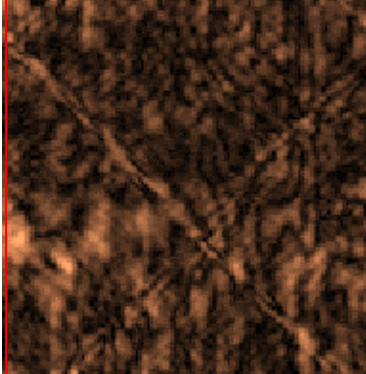
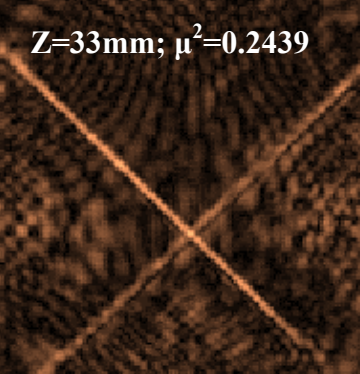
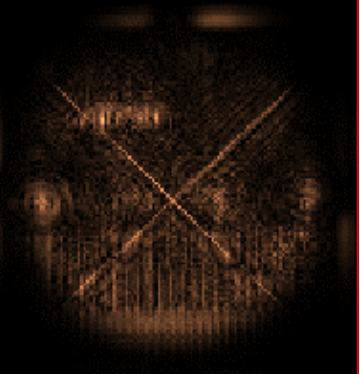
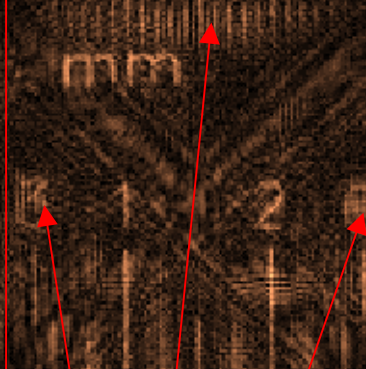
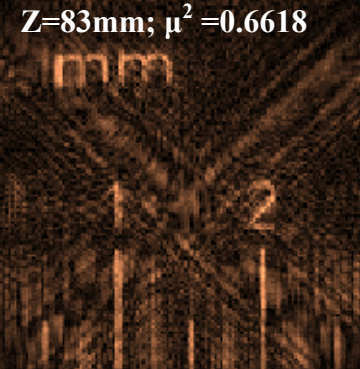
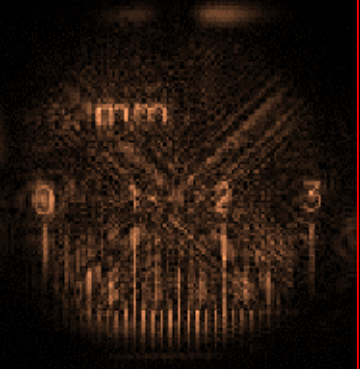
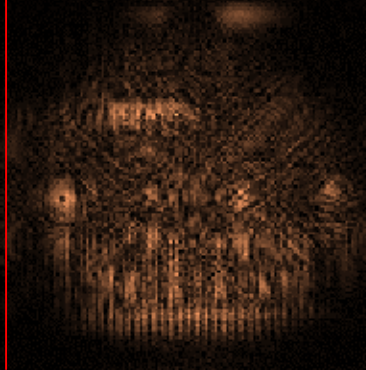
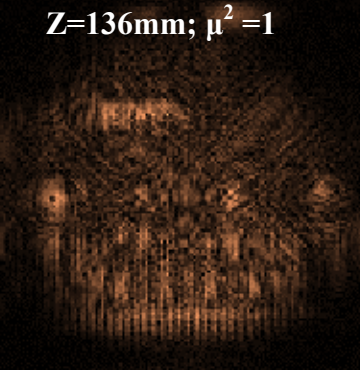
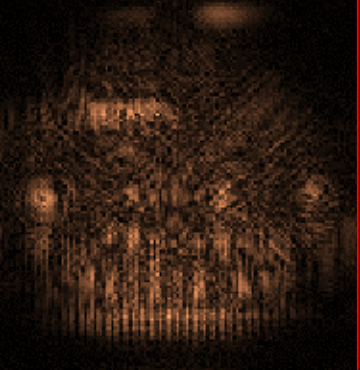
Fourier reconstruction algorithm	Free of aliasing reconstruction of the hologram central part by the Fourier algorithm	Convolution reconstruction algorithm
	<p>$Z=33\text{mm}; \mu^2=0.2439$</p> 	
Image is destroyed due to the aliasing	Magnified fragment of the object, no aliasing	
	<p>$Z=83\text{mm}; \mu^2=0.6618$</p> 	
Aliasing artifacts	Magnified fragment of the object, no aliasing	
	<p>$Z=136\text{mm}; \mu^2=1$</p> 	
All three reconstructions are identical		

Fig. 3.8. Three particular results of reconstruction of the Fresnel hologram of the test object shown in Fig. 3.7 for different values of the distance parameter μ^2 .

References

1. J. W. Goodman and R. W. Lawrence, Digital image formation from electronically detected holograms, *Applied Physics Letters*, August 1, 1967, Volume 11, Issue 3, pp. 77-79
2. M.A. Kronrod, N.S. Merzlyakov, L.P. Yaroslavsky, Reconstruction of a Hologram with a Computer, *Soviet Physics-Technical Physics*, v. 17, no. 2, 1972, p. 419 - 420.
3. L. P. Yaroslavskii, N.S. Merzlyakov, *Methods of Digital Holography*, Consultance Bureau, N.Y., 1980 (English translation from Russian edition: L. P. Yaroslavskii, N.S. Merzlyakov, *Methods of Digital Holography*, Moscow, Izdatel'stvo Nauka, 1977. 192 p.)
4. U. Schnars and W. Jüptner, Direct recording of holograms by a CCD target and numerical reconstruction, *Applied Optics*, Vol. 33, No. 2, 10 January 1994, pp. 179-181
5. E. N. Leith, J. Upatnieks, New techniques in wave front reconstruction, *JOSA*, 51, 1469-1473, 1961
6. I. Yamaguchi, T. Zhang, Phase-shifting digital holography, *Optics Letters*, Vol. 22, No. 16 / August 15, 1997, 1268-1270
7. J. Goodman, *Introduction to Fourier Optics*, McGraw-Hill, N.Y., 1996
8. L. Yaroslavsky, *Digital Holography and Digital Image Processing*, Kluwer Academic Publishers, Boston, 2004
9. L. Yaroslavsky, Shifted Discrete Fourier Transforms, in *Digital Signal Processing*, edited by V. Cappellini, Academic Press, London, 1980, p.69-74
10. L. R. Rabiner, R. W. Schafer, C. M. Rader, The chirp z-transform algorithm and its application, *Bell System Tech. J.*, 1969, Vol. 48: 1249-1292
11. Xuegong Deng, Bipin Bihari, Jianhua Gan, Feng Zhao, and Ray T. Chen, Fast algorithms for chirp transforms with zooming-in ability and its application, *J. Opt. Soc. Am. A*, Vol. 17, No. 4, April 2000
12. V. Namias, The Fractional Order Fourier Transform and its Applications to quantum mechanics, *J. Inst. Math. Appl.* v. 25, 241-265 (1980)
13. D. H. Bailey, P. N. Swartztrauber, The Fractional Fourier Transform and applications, *SIAM Rev.* 1991, Vol. 33, 389-404
14. L. Yaroslavsky and N. Ben David, Focal plane invariant algorithm for digital reconstruction of holograms recorded in the near diffraction zone, In: *Optical Measurement Systems for Industrial Inspection III*, SPIE's Int. Symposium on Optical Metrology, 23-25 June 2003, Munich, Germany, W. Osten, K. Creath, M. Kujawinska, Eds., SPIE v. 5144, pp. 142-149
15. L. Yaroslavsky, F. Zhang, and I. Yamaguchi, Point Spread Functions of digital reconstruction of digitally recorded holograms, In: *Information Optics and Photonics Technology*, SPIE v. 5144, Beijing, 142-149, (Jan. 2005), edited by Guoguang Mu, Francis T. Yu, Suganda Jatumila
16. I. S. Gradstein, I. M. Ryzhik, "Tables of integrals, series, and products", Academic Press, 1994.